



HAL
open science

Design and Optimization of a Dextrous Robotic Finger: Incorporating a Sliding, Rotating, and Soft-Bending Mechanism While Maximizing Dexterity and Minimizing Dimensions

Amir Pagoli, Frédéric Chapelle, Juan Antonio Corrales Ramon, Youcef
Mezouar, Yuri Lapusta

► To cite this version:

Amir Pagoli, Frédéric Chapelle, Juan Antonio Corrales Ramon, Youcef Mezouar, Yuri Lapusta. Design and Optimization of a Dextrous Robotic Finger: Incorporating a Sliding, Rotating, and Soft-Bending Mechanism While Maximizing Dexterity and Minimizing Dimensions. *IEEE Robotics and Automation Magazine*, 2020, 27 (4), pp.56-64. 10.1109/MRA.2020.3024283 . hal-03060366v1

HAL Id: hal-03060366

<https://uca.hal.science/hal-03060366v1>

Submitted on 13 Dec 2020 (v1), last revised 5 Feb 2021 (v2)

HAL is a multi-disciplinary open access archive for the deposit and dissemination of scientific research documents, whether they are published or not. The documents may come from teaching and research institutions in France or abroad, or from public or private research centers.

L'archive ouverte pluridisciplinaire **HAL**, est destinée au dépôt et à la diffusion de documents scientifiques de niveau recherche, publiés ou non, émanant des établissements d'enseignement et de recherche français ou étrangers, des laboratoires publics ou privés.



Distributed under a Creative Commons Attribution 4.0 International License

Design and Optimization of a Soft Reconfigurable Robotic Finger with a Sliding and Bending Pneumatic Actuator

A. Pagoli, F. Chapelle, J. Corrales, Y. Mezouar, Y. Lapusta

Abstract— In this paper, a new soft finger with a pneumatic-actuated movable joint is introduced, optimized and characterized in terms of degrees of freedom, workspace and fingertip force. The finger mainly consists of one soft link as the body and one soft joint as the bending actuator. Due to the additional translation and rotation movement capabilities of the joint carried out by two stepper motors, the finger can bend in any direction while having different lengths. This not only results in more flexibility of the finger dealing with obstacles limiting the workspace but also increases the possible configurations in which the finger can reach and exert force to any specific point in the 3D space. Regulating the air pressure in the hollow space inside the link, the stiffness of the finger and consequently the applied force can vary up to two times. Finite element analysis was used to optimize the joint geometry in order to maximize the bending angle and minimize the joint dimensions. Furthermore, the variations of each design parameter and the consequent effects on the optimization objectives were analyzed. The optimized values of geometrical parameters were then utilized to fabricate a prototype with silicone rubber. Bending angle and tip force tests were conducted on the prototype in order to validate the numerical modeling. The experimental results showed that the finger can exert force up to 650 mN.

Index Terms— soft robots, fluidic elastomer actuation, FEM analysis, dexterity, movable joint

I. INTRODUCTION

Introduced as a novel technology in recent years, soft robotics broadens new horizons in the field of robotics thanks to promising characteristics such as adaptability, lightweight, less assembly and low cost. Although conventional robots with rigid structures are designed to perform high-precision tasks in a large variety of environments, there are still lots of challenges in handling objects with diverse sizes, shapes, and properties which stem from intrinsic restrictions such as insufficient DOFs (Degrees of Freedom) in a given workspace. Initially, overcoming these limitations, a new branch of robots, known as hyper-redundant robots, were introduced with a large number of joints which increases their DOFs and eventually tailored them to work in unstructured environments with high dexterity; nevertheless, this abundance of joints complicates the process of control [1]. The emergence of soft robots addressed this problem due to the intrinsic compliant shape, passive adaptation, small

number of actuators and high DOFs. Inspired from nature, the compliant essence of soft robots brings about a whole range of novel special utilizations. Most of these applications concern safely interacting with uncertain and dynamic task environments, such as handling objects with diverse characteristics or maneuvering through congested spaces with the least amount of stress concentrations or damaging.

The intrinsic deformable structure of soft robots encourages scientists to engage different technologies for their dynamization. One of the most widely used actuating technologies is FEA (Fluid Elastomer Actuation), powered by a pressurized fluid (gas or liquid) [2]. FEAs have been used in numerous configurations for diverse purposes such as locomotion [3], manipulation [4], medical applications [5] and wearable devices [6]. These actuators can generate distributed forces which are proportional to the pressure of the fluid and the surface area on which the active pressure is applied [7]. Even though there is a large diversity of applications for FEAs, many challenges still remain in this field including stiffness and bending shape control. Many researches have been conducted to increase the performance of these kinds of actuators by integrating them with other types of actuation methods which help FEAs in term of shape control. These lateral technologies are mainly based on using variable stiffness materials including shape memory polymers (SMP) [8], combination of SMP and thermoplastic polyurethane (TPU) [9], and low melting point alloys (LMPA) [10]. The main drawbacks of SMPs are low actuation speed and high hysteresis; however, some improvements have been reported in these areas recently [11-12]. Using low melting point alloy (LMPA) is another suggested method for changing bending point and shape configuration in FEAs. Applying electric current to the alloy and heating it makes the structure phase to change from rigid to soft, and thus variable stiffness can be achieved [13]. Like SMPs, the transition time is the main issue in LMPAs. Depending on size and geometry, melting time for LMPAs differs from 1 to 30 s, while cooling takes over 60 s [14].

In this article, a novel type of soft finger is introduced (Figure 1), consisting of one elastomer tube as the soft link and one movable soft joint as the actuator. Applying the air pressure to the joint, the joint and the link will bend concurrently. Moving longitudinally along the finger as well as rotating around it, the joint can change the effective length of the finger and also the bending direction. This results in more possible configurations in which the finger can reach any specific point in 3D space; besides, due to the pressure regulation mechanism connected to the link, the stiffness of the link can be altered which leads to applying the proper amount of force at the tip point of the finger in each configuration.

The authors are with Université Clermont Auvergne, CNRS, SIGMA Clermont, Institut Pascal, F-63000 CLERMONT-FERRAND, FRANCE.
Emails: {amir.pagoli, frederic.chapelle, juan-antonio.corrales-ramon, youcef.mezouar, yuri.lapusta}@sigma-clermont.fr

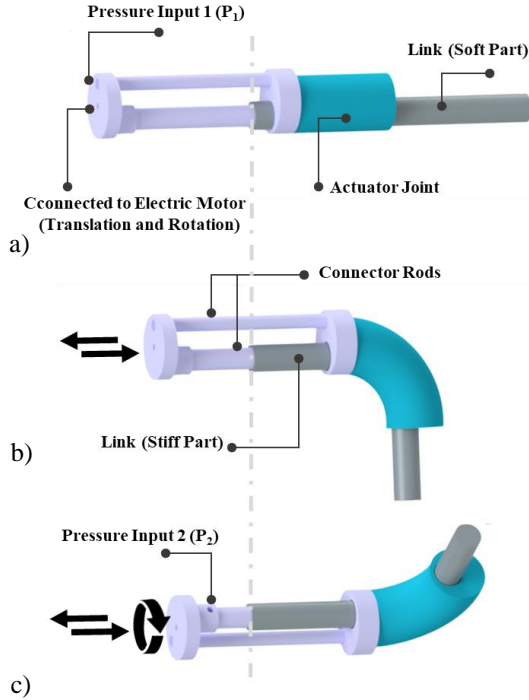


Fig. 1. a) Schematic view of the proposed finger. b) sliding the joint along the link and changing the bending point and the effective length of the finger. c) rotation of the joint along its axis which results in changing the bending direction in 3D space.

The following section of the article discusses the conceptual and structural design of the proposed finger. section III explains the optimization process. The fabrication procedure is introduced in section IV. Numerical validation and experimental results are presented in section V followed by conclusions and discussions about the future work.

II. OPERATING PRINCIPLES AND DESIGN

The schematic of the proposed soft finger is illustrated in Figure 1. The finger is composed of a pneumatically actuated joint and a soft link. (Figure 1a). A longitudinal channel is embedded inside the joint which inflates by supplying the air pressure and leads to the bending of the joint and consequently the link. The bending location can be longitudinally changed by sliding the joint along the link (Figure 1b). The joint can also rotate around its main axis while the link remains steady due to its fixed connection to the base. This causes the finger to bend in any direction in 3D space (Figure 1c).

In Figure 2, a conventional FEA finger (on the right) and the proposed finger (on the left) are compared in terms of dexterity and the strategies to reach a particular point in the workspace. Due to the uniform structure of the conventional FEA fingers and their limited degree of freedom, it is not possible for them to attain each point in their workspace with various configurations. On the contrary, the design of the proposed finger suggests an array of possible configurations in which the finger can reach each point. This not only results in more flexibility of the finger in dealing with obstacles that limit the workspace but also enhances the possible configurations in which the finger can exert force to a

particular point. In addition, unlike the conventional FEAs, the new design can rotate and change the direction of bending. This along with the translational movements of the bending point result in a 3D workspace and thus more accessible points around it.

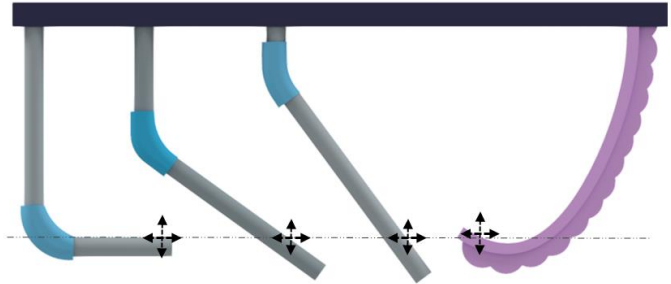


Fig. 2. Comparison between the configurations of the proposed finger (left) and a conventional FEA-based finger (right) for reaching a particular point.

The mechanism used for changing the bending point of the finger mainly consists of two stepper motors connected to the joint; The first stepper motor is linked directly to the joint and is responsible for its rotational displacement. The connection includes two rigid rods; one for transmitting the rotational movement of the motor to the joint, and the other with a tubular shape passing through the center of the link, for enhancing the stiffness of the region behind the joint which facilitates its deformation and improves its controllability. As for linear longitudinal movement of the joint, the assembly of the joint and the first motor is entirely displaced by the second stepper motor using a ball screw mechanism (Figure 3).

Two air streams with different pressures are supplied to the finger; P_1 which deforms the joint and P_2 which regulates the stiffness of the link. These two air streams are applied to the joint and the link via the two aforementioned rigid rods between the joint and the first stepper motor.

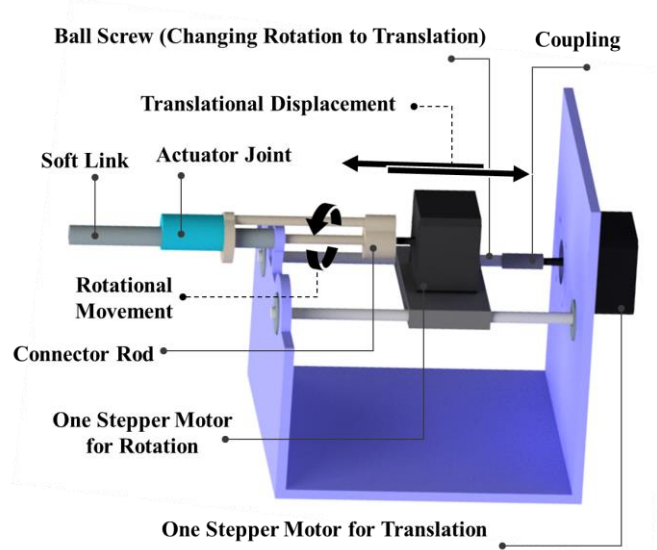


Fig. 3. Assembly structure of the proposed finger and the motors

III. DESIGN OPTIMIZATION

In this section, the optimization procedure is described for a finger with the approximate dimensions of the human finger (diameter=10 mm and length=150 mm). The objective of the optimization is to find the best values of the design parameters in order to meet the design objectives; i.e., maximizing the bending angle of the finger (θ) and minimizing the joint dimensions (length and diameter) under an approximate value of applied pressure to the joint (P_1).

The amount of this pressure is determined based on the 80% of the pressure that causes the joint to burst with 1 mm thickness of the chamber wall (H_1) which is equal to 14 kPa.

Figure 4 summarizes the design parameters under investigation including the main geometrical parameters of the joint. The range of variation for each design parameter is tabulated in Table I. The lower and the upper bounds are specified based on the fabrication considerations and also the dimensions of the finger which are expected to be equivalent to the human finger. The pressure inside the link (P_2) is taken into account as another design parameter and the minimum value is selected in a way that a sensible variation is observed in the stiffness of the finger.

To optimize the parameters, a comprehensive analysis should be conducted in the specified ranges. Finite Element Analysis is employed to numerically solve the relevant equations for the flexible materials. ANSYS Workbench package with the option of nonlinear large deformation analysis for hyperelastic materials is used as the framework for solving these numerical equations and performing optimizations, simultaneously.

As for selecting the materials, two variations of platinum catalyzed silicones are nominated to fabricate the actuator module; Ecoflex 00-30 and 00-50, the code numbers referring to the material's shore hardness. As studied by Elsayed et al. [15], both the silicones exhibited the same bending behavior, however, lower pressure is required to deform the joint made of Ecoflex 00-30; accordingly, in this work, this material is selected to fabricate the joint. As for the link, Dragonskin 00-30 is selected. This is due to the direct interaction of the link with objects and consequently the need for higher stiffness. Simulating the behaviors of these materials, silicone rubber is presumed as an isotropic and hyperplastic material which simplifies the general polynomial form of the strain energy potential into:

$$U = \sum_{i+j=1}^N C_i (\bar{I}_1 - 3)^i (\bar{I}_2 - 3)^j + \sum_{i=1}^N \frac{1}{k_i} (J_{el} - 1)^{2i} \quad (1)$$

where U is the strain energy potential per unit volume, N is the polynomial order, \bar{I}_1 and \bar{I}_2 are the deviatoric strain invariants, C_i is a material specific parameter, J_{el} is the elastic volume ratio and k_i expresses compressibility.

Considering the silicone as an incompressible material, the term k_i is omitted. The third order Ogden model ($N=3$) for the strain energy potential is expressed with λ and α as the empirical parameters (2). According to [16], for the Ecoflex 00-30, the parameter values $\mu_1 = 22$ kPa,

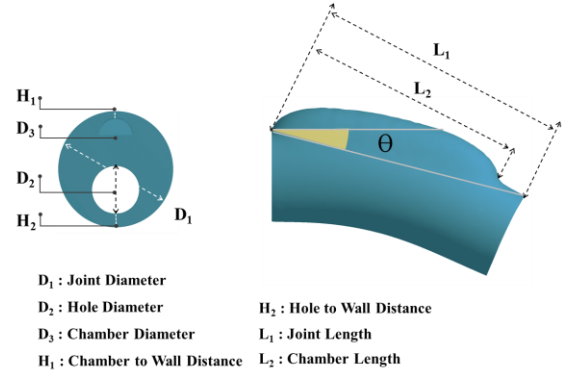


Fig. 4. The geometrical optimization parameters

TABLE I. RANGES FOR DESIGN OPTIMIZATION PARAMETERS

Design Parameters	Lower Bound	Upper Bound
Joint length - L_1 (mm)	40	60
Chamber length - L_2 (mm)	30	50
Joint Diameter - D_1 (mm)	20	40
Chamber Diameter - D_2 (mm)	6	10
Chamber Wall thickness - H_1 (mm)	1	2
Hole Wall thickness - H_2 (mm)	1	5
Pressure inside the link - P_2 (kPa)	110	150

$\alpha_1 = 1.3$, $\mu_2 = 0.4$ kPa, $\alpha_2 = 5$, $\mu_3 = -2$ kPa and $\alpha_3 = -2$ J/m³ show the best curve fit with the experimental stress-strain data of the mechanical tests.

$$U = \sum_{i=1}^N \frac{2\mu_i}{\alpha_i^2} (\lambda_1^{\alpha_i} + \lambda_2^{\alpha_i} + \lambda_3^{\alpha_i} - 3) \quad (2)$$

As for Dragon skin 00-30, the second order Yeoh model is chosen due to the promising fitting with the stress-strain data of the mechanical tests with the parameter values of $N = 2$, $C_{10} = 1.190$ kPa and $C_{20} = 23.028$ kPa [17]. This model can be presented for incompressible materials as in (3).

$$U = C_{10} (\bar{I}_1 - 3) + C_{20} (\bar{I}_1 - 3)^2 \quad (3)$$

Due to the large deformations in the joint structure, SOLID187 elements are used to mesh the model. These elements with quadratic displacement behavior are defined by ten nodes having three degrees of freedom at each node. This characteristic along with capabilities such as plasticity, hyperelasticity, creep, stress stiffening, large deflection, and large strain make them well suited to model irregular meshes (such as those produced in this analysis). Owing to symmetrical pattern of the link, the meshing process is performed using the elements of type SOLID186 which are defined by 20 nodes with three degrees of freedom per node. These elements exhibit quadratic displacement behavior with isotropic material properties and similar to the elements of type SOLID187, they support different capabilities regarding large deflections. As for the contact pairs, CONTAC174 and

TARGE170 are chosen. Fixed support boundary conditions are applied to the beginning of both the link and the joint while the tips are set free to move. As for simulating the pressures in the joint and the link chambers (P_1 & P_2), constant normal pressure boundary conditions are considered with relevant values. Figure 5 illustrates the results of bending simulation of a sample up to 90 degrees under the actuation pressure of 14 kPa.

Due to the multiple number of design parameters, objectives and constraints, the Adaptive Multiple-Objective optimization method is selected to find the global optimum parameters. This method is a type of the NSGA-II (Non-dominated Sorted Genetic Algorithm-II) which is based on controlled elitism concepts [18]. The goal is to maximize the bending angle up to 90 degrees and simultaneously minimizing the length and diameter of the joint under different values of the applied pressure to the joint (P_1) around 14 kPa. This average value is selected through trial and error so that the finger with the specified ranges of geometrical dimensions can bend up to 90 degrees and not to burst. The calculation converged after 146 evaluations by generating 400 samples with 50 samples per iteration and finding 3 candidates. Figure 6a presents the local sensitivity of the final optimized result to each design parameter in

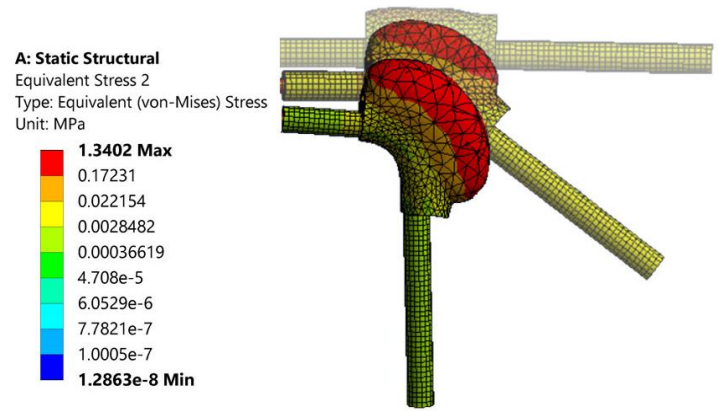
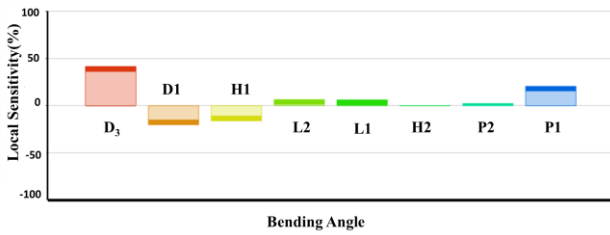
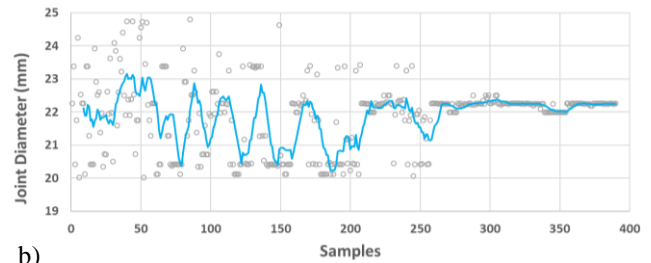


Fig. 5. FEA simulation of a finger up to 90 degrees

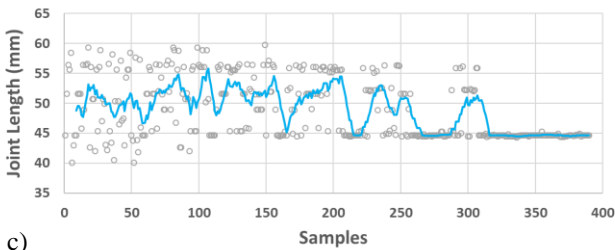
percent. This parameter shows the norm of the partial derivatives of the finger bending angle with respect to the selected design parameters. As it can be observed, the chamber diameter (D_3) and the actuation pressure (P_1) are estimated to be the most influential elements with direct relation to the bending angle in the sensitivity analysis; in



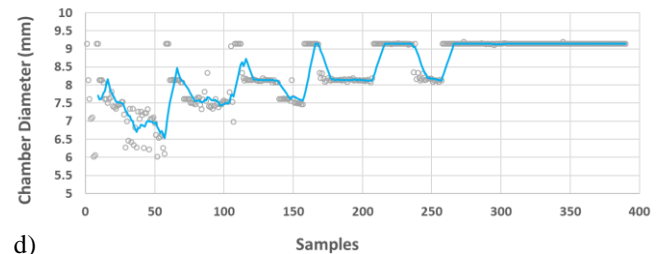
a)



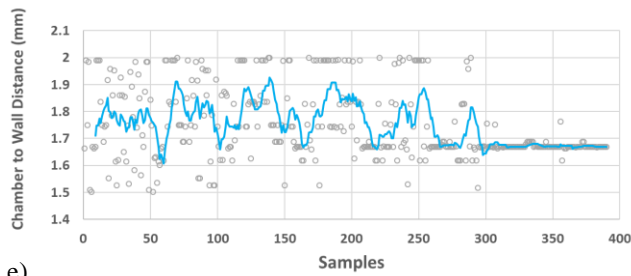
b)



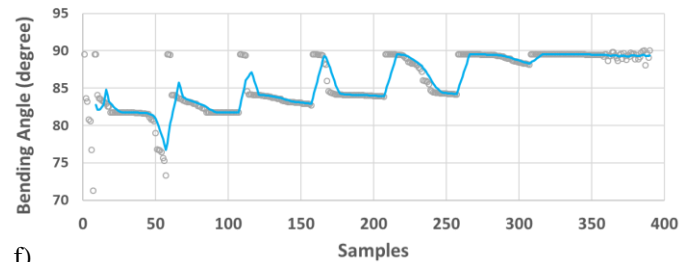
c)



d)



e)



f)

Fig. 6.a) local sensitivity of the optimized result to each design parameter. b-f) convergence of the design parameters to the final optimized values

other words, compared to other variables, increasing these two elements results in more intense positive changes in the final bending angle. The joint diameter (D_1) and the chamber to wall distance (H_1) stand in the next ranks of the most effective parameters, but in reverse relation with the main objective which means that the reduction in the values of these parameters causes the final bending angle to increase. On the other hand, the variations of the hole wall distance (H_2) and the pressure inside the link (P_2) are estimated to be almost ineffective to the main objectives of the optimization and hence to be neglected, nevertheless, it should be noted that P_2 is an important parameter for changing the finger stiffness and thus the applied fingertip force. The effect of this parameter will be discussed in the following of this paper. As for H_2 , the value is determined according to manufacturing considerations and is set to 2 mm. The low value of this parameter would result in aligning the surfaces of the joint and the link in the bending direction. This eventually leads to a uniform smooth surface in that area which can be beneficial in future possible grasping applications.

As for the rest of design parameters, the optimization procedures are illustrated in Figures 5b-5f. In these figures, the values of parameters in each sample are shown with empty circles and the blue lines which are the moving average of the values represent the general trend of convergence to the optimized numbers. Table II summarizes the eventual optimized values of the design parameters.

TABLE II. FEM OPTIMIZED PARAMETERS

<i>Design Parameters</i>	<i>Optimized value</i>
Joint length - L_1 (mm)	44.6
Chamber length - L_2 (mm)	42.5
Joint Diameter - D_1 (mm)	22.5
Chamber Diameter - D_2 (mm)	9.14
Chamber to Wall thickness - H_1 (mm)	1.68

These dimensions will be used to manufacture the prototype of the finger which will be described in the following sections.

IV. MANUFACTURING AND FABRICATION PROCESS

In this section, the fabrication procedure of the soft finger with the optimized dimensions is described. Both the link and the joint are manufactured using mold casting process (Figure 7). The molds are printed with the Ultimaker3 3D printer. Thanks to recent advances in 3D printing technology, the fabrication process of soft components has been facilitated significantly which leads to producing more complex parts with higher precision. In this work, the resolution of the printer is set around 20 microns and thus the process of printing all the molds lasts for about 20 hours.

For each silicone, two liquid parts should be mixed with the same ratio followed by 2-3 minutes vacuum degassing in order to eliminate any entrapped air bubbles. This will be done by placing the molds in a vacuum chamber. The normal cure time of Eco-Flex 00-30 is around 4 hours in ambient temperature which can be reduced to less than an hour by putting it in the oven at the temperature of 100°C.

V. RESULTS AND DISCUSSION

Validating the numerical model introduced in the previous sections, the fabricated finger undergoes two sets of experiments; i.e., bending and force tests. Figure 8 illustrates the prototype assembled to conduct the experimental tests. Controlling the whole process including reading sensors, managing switches, and handling electric motors is performed by an Arduino Uno board which is connected to the computer via a USB wire. A 12V 350 kPa air pump is used for supplying the pressurized air for the system. Regulating the pressures P_1 and P_2 independently, one solenoid valve and one silicon piezoresistive pressure sensor are embedded in each air stream. The feedback signals transferred from each pressure sensor to the Arduino are used to switch on and off the air pump and the relevant solenoid valve. Two test benches have been developed to characterize the bending angle as well as the blocking force of the fingertip. The bending angle of the finger is visually checked using a printed protractor placed at the joint's center of bending (Figure 8b). As for measuring the force applied by the fingertip, a force sensor is situated below the tip point of the finger and directly transfers the force data to the computer (Figure 8c). Due to the weight of the link, at initial state, a deflection of 10 degrees at the tip point of the finger can be observed which will be resolved by applying the pressure P_2 inside the link.

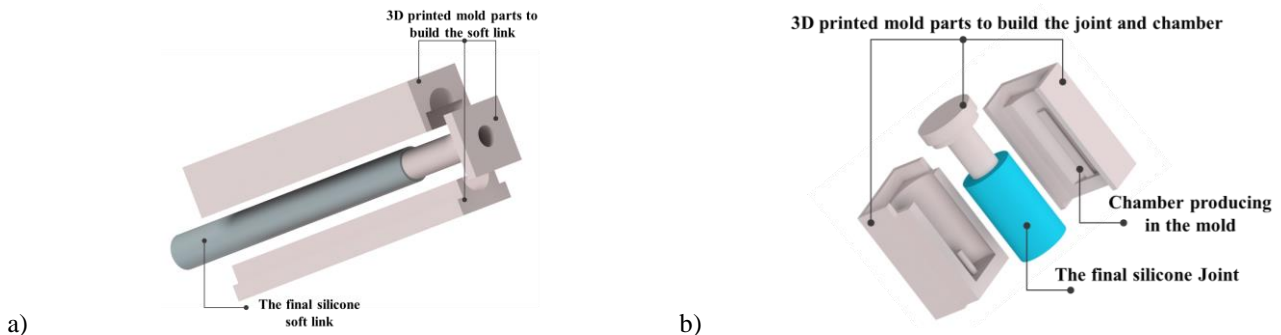


Fig. 7. Mold design of the soft finger, a) the soft link b) the joint with one chamber

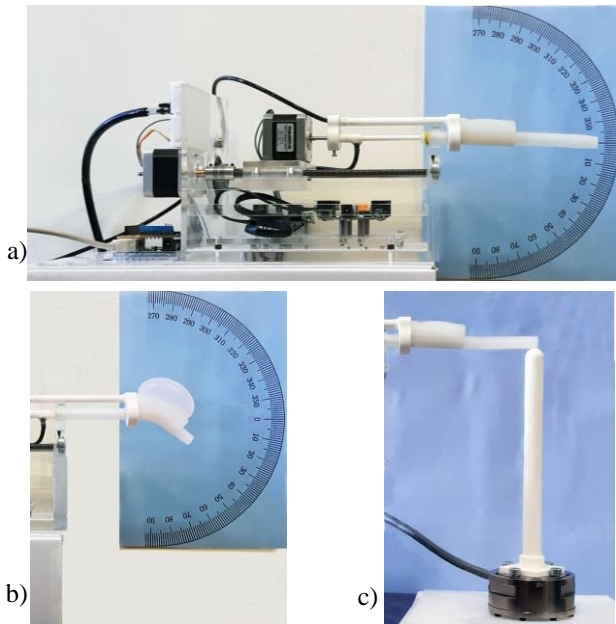


Fig. 8. a) The overall view of the assembled prototype, b) Test bench for measuring the joint angle. c) Test bench for measuring the fingertip force

Different pressures are applied to the finger and the consequent bending angles are measured (Figure 9a). These angles are compared with the numerical results in Figure 9b. It can be noticed that there is an acceptable agreement between the experimental and numerical data which can be taken as the validity of the model and thus the optimization results. As the second test with the assembled prototype, the force at the tip point of the finger is measured as a function of

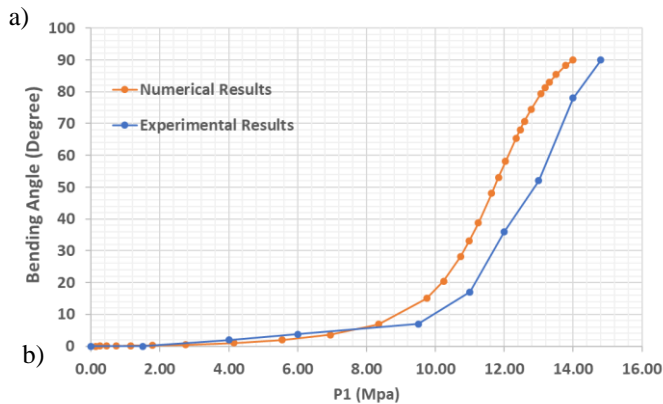
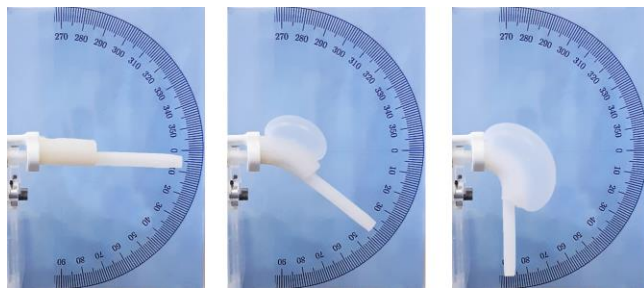


Fig. 9. a) Bending of the prototype under different applied pressures. b) The comparison between the numerical and experimental bending angles as a function of applied pressure

different parameters including longitudinal position of the joint and the stiffening pressure (P_2). All the tests are conducted under the actuation pressure of 14 kPa. The results are presented in Figure 10. As illustrated, by changing the position of the joint toward the tip of the finger, the applied force increases by almost 3 times. Furthermore, applying the pressurized air into the link results in higher stiffness and thus higher amount of force up to 650 mN which is twice the initial value.

The wide interval of fingertip force along with the diversity of configurations to reach a particular point lead to various strategies the finger can undertake dealing with different situations such as low or high amount of required force or the presence of any obstacle in the workspace.

VI. CONCLUSION

In this paper, a new innovative variable stiffness soft finger with a fluid-actuated movable joint has been introduced and optimized in terms of its main characteristics. The finger mainly consists of one soft sliding joint as the bending actuator and a soft link as the body. Applying pressurized air into the joint's chamber, the joint and consequently the link will bend in a specific direction. The location and the direction of the bending can be changed by sliding the joint longitudinally along the link and also rotating it around its main axis which are carried out using two electric motors. The variable length of the finger and the capability of bending in different directions result in diversity of configurations the finger can reach a point and exert force, and thus higher dexterity. Optimization over different

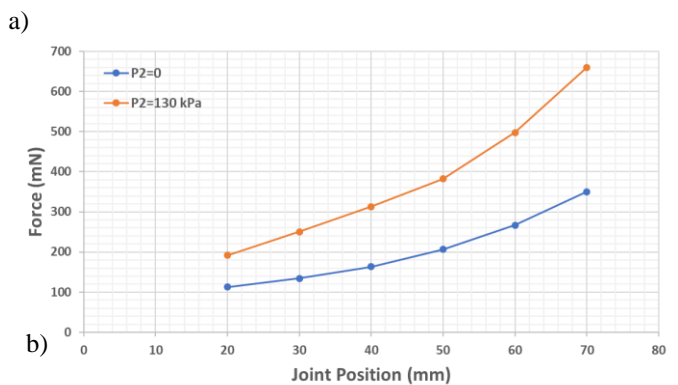
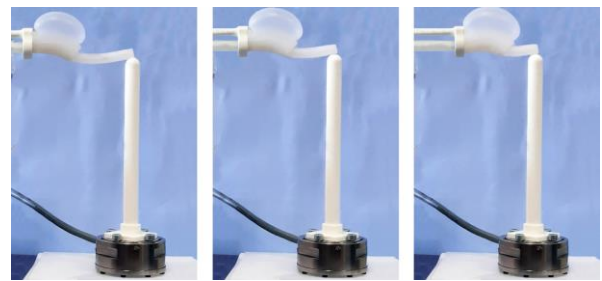


Fig. 10. Fingertip force test results as a function of the stiffening pressure (P_2) and the joint longitudinal position

parameters involved in the problem was performed in order to minimize the joint dimensions and also maximize the bending angle of the finger. In addition, the sensitivity of each design parameter on the optimization objectives were analyzed. The final optimized geometrical parameters were used for fabricating a prototype which was used to validate the numerical model. Another experiment was also designed to study the amount of force applied by the fingertip. It was shown that the longitudinal location of the joint and also the pressure inside the link (P_2) are highly effective to this force. In a particular configuration, the finger can exert force up to 650 mN.

For the future work, we are going to address the problem of ballooning effect of the chamber which is responsible for possible bursting of the joint. Furthermore, the idea of using these fingers to make a dexterous gripper with manipulation capabilities will be studied.

ACKNOWLEDGMENT

This work has been sponsored by the French government research program “Investissements d’Avenir” through the IDEX-ISITE initiative 16-IDEX-0001 (CAP20-25).

REFERENCES

- [1] D. Trivedi, C. D. Rahn, W. M. Kier, and I. D. Walker, “Soft robotics: Biological inspiration, state of the art, and future research,” *Applied bionics and biomechanics*, vol. 5, no. 3, pp. 99–117, 2008.
- [2] A. D. Marchese and D. Rus, “Design, kinematics, and control of a soft spatial fluidic elastomer manipulator,” *The International Journal of Robotics Research*, vol. 35, no. 7, pp. 840–869, 2016.
- [3] R. F. Shepherd *et al.*, “Multigait soft robot,” *Proceedings of the national academy of sciences*, vol. 108, no. 51, pp. 20400–20403, 2011.
- [4] W. McMahan *et al.*, “Field trials and testing of the OctArm continuum manipulator,” in *Proceedings 2006 IEEE International Conference on Robotics and Automation, 2006. ICRA 2006.*, 2006, pp. 2336–2341.
- [5] M. Cianchetti, T. Ranzani, G. Gerboni, I. De Falco, C. Laschi, and A. Menciassi, “STIFF-FLOP surgical manipulator: mechanical design and experimental characterization of the single module,” in *Intelligent Robots and Systems (IROS), 2013 IEEE/RSJ International Conference on*, 2013, pp. 3576–3581.
- [6] P. Polygerinos, Z. Wang, K. C. Galloway, R. J. Wood, and C. J. Walsh, “Soft robotic glove for combined assistance and at-home rehabilitation,” *Robotics and Autonomous Systems*, vol. 73, pp. 135–143, 2015.
- [7] H. K. Yap, H. Y. Ng, and C.-H. Yeow, “High-force soft printable pneumatics for soft robotic applications,” *Soft Robotics*, vol. 3, no. 3, pp. 144–158, 2016.
- [8] Y. Yang, Y. Chen, Y. Li, M. Z. Chen, and Y. Wei, “Bioinspired robotic fingers based on pneumatic actuator and 3D printing of smart material,” *Soft robotics*, vol. 4, no. 2, pp. 147–162, 2017.
- [9] Y. Yang, Y. Chen, Y. Li, Z. Wang, and Y. Li, “Novel variable-stiffness robotic fingers with built-in position feedback,” *Soft robotics*, vol. 4, no. 4, pp. 338–352, 2017.
- [10] Y. Hao *et al.*, “A eutectic-alloy-infused soft actuator with sensing, tunable degrees of freedom, and stiffness properties,” *Journal of Micromechanics and Microengineering*, vol. 28, no. 2, p. 024004, 2018.
- [11] H. Lu, Y. Liu, J. Gou, J. Leng, and S. Du, “Synergistic effect of carbon nanofiber and carbon nanopaper on shape memory polymer composite,” *Applied Physics Letters*, vol. 96, no. 8, p. 084102, 2010.
- [12] M. Behl, M. Y. Razzaq, and A. Lendlein, “Multifunctional shape-memory polymers,” *Advanced materials*, vol. 22, no. 31, pp. 3388–3410, 2010.
- [13] H. K. Yap, J. H. Lim, F. Nasrallah, J. C. Goh, and R. C. Yeow, “A soft exoskeleton for hand assistive and rehabilitation application using pneumatic actuators with variable stiffness,” in *2015 IEEE international conference on robotics and automation (ICRA)*, 2015, pp. 4967–4972.
- [14] B. E. Schubert and D. Floreano, “Variable stiffness material based on rigid low-melting-point-alloy microstructures embedded in soft poly (dimethylsiloxane)(PDMS),” *Rsc Advances*, vol. 3, no. 46, pp. 24671–24679, 2013.
- [15] Y. Elsayed, C. Lekakou, T. Geng, and C. M. Saaj, “Design optimisation of soft silicone pneumatic actuators using finite element analysis,” in *2014 IEEE/ASME International Conference on Advanced Intelligent Mechatronics*, 2014, pp. 44–49.
- [16] D. Steck, J. Qu, S. B. Kordmahale, D. Tscharnuter, A. Muliana, and J. Kameoka, “Mechanical responses of Ecoflex silicone rubber: Compressible and incompressible behaviors,” *Journal of Applied Polymer Science*, vol. 136, no. 5, p. 47025, 2019.
- [17] Y. Elsayed *et al.*, “Finite element analysis and design optimization of a pneumatically actuating silicone module for robotic surgery applications,” *Soft Robotics*, vol. 1, no. 4, pp. 255–262, 2014.
- [18] K. Deb, A. Pratap, S. Agarwal, and T. Meyarivan, “A fast and elitist multiobjective genetic algorithm: NSGA-II,” *IEEE transactions on evolutionary computation*, vol. 6, no. 2, pp. 182–197, 2002.